Cooperative cell invasion: matrix metalloproteinase–mediated incorporation between cells

Camilla B. Mitchell[a] and Geraldine M. O'Neill[a,b,*]
[a]Children's Cancer Research Unit, Kids Research Institute, Children's Hospital at Westmead, Westmead, NSW 2145, Australia; [b]Discipline of Child and Adolescent Health, University of Sydney, Sydney, NSW 2006, Australia

ABSTRACT **Progression to metastatic disease is a leading cause of cancer death. Tumors are a complex mixture of cell types, both genetically heterogeneous malignant cells and associated nonmalignant cells. Models mimicking this heterogeneous cell environment have revealed that invasive cell populations can induce dissemination by otherwise poorly/noninvasive tumor cells, known as cooperative invasion. Neuroblastoma tumors arise in children and are characterized by mixed cellular populations in vivo, consisting chiefly of neuronal (N)-type and substrate (S)-type cells. The S-type cells have all the hallmarks of invasive leader cell populations and have been coisolated with N-type cells from metastatic bone lesions, but to date their ability to induce cooperative invasion has not been investigated. Therefore, in the present study, we analyzed the invasive behavior of mixed N-type and S-type multicellular spheroids embedded in three-dimensional collagen gels. Our analyses show that S-type cells induce invasion of either single cells or small cell clusters of N-type cells. In contrast to other reports of cooperative invasion in which mixed cultures exhibit a follow-the-leader mechanism, we show coincident emergence of S- and N-type cells from mixed spheroids. Our data suggest mutual effects between the two cell types. Thus, whereas coculture with S-type cells induces N-type invasion, coculture with N-type cells slows S-type invasion. Using matrix metalloproteinase (MMP) inhibitors and cell incorporation assays, we demonstrate that MMP activity is required for S-type cells to insert into layers of N-type cells. Our study therefore highlights an important role for S-type neuroblastoma cells in the invasion process and reveals a new mechanism of cooperative invasion.**

Monitoring Editor
Valerie Marie Weaver
University of California, San Francisco

Received: Mar 24, 2016
Revised: Aug 26, 2016
Accepted: Aug 30, 2016

INTRODUCTION

Cooperative invasion describes how inherently invasive cells, either malignant or nonmalignant, can induce invasion of otherwise poorly invasive subpopulations in mixed cell populations in tumors (Gaggioli *et al.*, 2007; Wyckoff *et al.*, 2007; DeNardo *et al.*, 2009; Dang *et al.*, 2011; Carey *et al.*, 2013; Cheung *et al.*, 2013; Chapman *et al.*, 2014; Etienne-Manneville, 2014; Westcott *et al.*, 2015). It is increasingly realized that tumors consist of heterogeneous cell populations, thus suggesting that cooperative invasion mechanisms may be important in the progression to metastatic cancer. The pediatric tumor neuroblastoma is characterized by mixed cell populations and the development of metastatic disease. In the present study, we therefore investigated cooperative invasion mechanisms between neuroblastoma cell subtypes.

During cooperative invasion, a "leader" cell population frequently initiates invasion into the surrounding matrix, and follower cells subsequently invade. The leader cells are characteristically highly migratory, with rapidly protrusive leading edges, whereas the follower cells often invade as collective multicellular strands behind

This article was published online ahead of print in MBoC in Press (http://www.molbiolcell.org/cgi/doi/10.1091/mbc.E16-03-0194) on September 7, 2016.
*Address correspondence to: Geraldine M. O'Neill (geraldine.oneill@health.nsw.gov.au).
Abbreviations used: BrdU, bromodeoxyuridine; MCS, multicellular spheroids; MMP, matrix metalloproteinase; N, neuroblastic; S, stromal.

the leader cells (Carey *et al.*, 2013). In one mechanism, the invasive or leader cell provides a factor in-*trans*, such as matrix metalloproteinase (MMP), which creates a path through the three-dimensional (3D) matrix for follower cells (Carey *et al.*, 2013; Chapman *et al.*, 2014). In another mechanism, invasion-inducing cells may instead simply create paths in the matrix by exerting force on collagen fibers and thereby create invasion cues to the second cell population (Dang *et al.*, 2011). Alternatively, the invasive cells create paths via a combination of protease- and force-mediated matrix remodeling (Gaggioli *et al.*, 2007) or through deposition of additional extracellular matrix components (Chapman *et al.*, 2014). Specific GTPase activity is a feature of the invasion inducer cells, but the GTPases that are required differ between tumor types (Carey *et al.*, 2013; Westcott *et al.*, 2015). Furthermore, the invasion-inducer cells can in turn be altered by the cooperative interaction. For example, previously protease-independent invaders were observed to switch to a protease-dependent mode of invasion during cooperative invasion (Chapman *et al.*, 2014). Such changes in invasive modes may ultimately determine subsequent routes of metastatic dissemination (Giampieri *et al.*, 2009).

Neuroblastoma tumors arise from cells of neural crest origin and are the most common extracranial solid tumor in children. They can occur anywhere along the sympathetic nervous system, but most commonly appear in the adrenal gland. Individual tumors frequently constitute mixed cell types including both neuroblastic (N) and stromal (S) cell types (Mora *et al.*, 2001; Mora and Gerald, 2004). Cell lines representing each of these phenotypes have been isolated from patient tumors (Ross *et al.*, 2003). The S-type cells have many features in common with fibroblasts, including elongated Rac-dependent 3D invasion (Zhong *et al.*, 2014). The coisolation of S- and N-type neuroblastoma cells from metastatic bone tumors (Valent *et al.*, 1999, 2001) suggests that cooperative invasion may occur in neuroblastoma, but this has not previously been investigated. In the present study, we used multicellular spheroids of mixed N- and S-type neuroblastoma cells cultured in 3D collagen to assess cooperative invasion.

RESULTS

SK-N-SH spheroids exhibit mixed invasion

We first analyzed invasive phenotypes in the SK-N-SH neuroblastoma line, which is an example of a cell line isolated as a mixed population of S- and N-type cell subtypes (Ciccarone *et al.*, 1989). We determined that the culture retained subtype heterogeneity, by immunostaining for the canonical S-type marker CD44 (Gross *et al.*, 1994; Figure 1A). To confirm specificity of this staining, we separately analyzed CD44 immunoreactivity in S-type SHEP and N-type SH-SY-5Y neuroblastoma lines, which were established from the parental SK-N-SH line (Thiele, 1998) and a second N-type line IMR32. This confirmed that the S-type SHEP cells are positive for CD44, whereas both N-type lines are negative. Next analysis of collagen-embedded SK-N-SH multicellular spheroids (MCS) revealed both collective and single-cell invasion: multicellular strands (Figure 1B, arrowheads) and, beyond the end of the strands, individual elongated cells (Figure 1B, arrows). SK-N-SH MCS have a tight core with prominent cell–cell adhesions as revealed by the cobblestone appearance of actin immunostaining (Figure 1C). The single elongated invasive cells that invade into the collagen are CD44 positive (Figure 1D), as are cells at the MCS periphery, which extend elongated membrane processes into the surrounding matrix (Figure 1D, arrows). This indicates that individual invasive cells represent the S-type fraction of SK-N-SH cells. Collectively these data suggested that S-type cells may be "leader" cells.

Coculture of neuroblastoma subtypes changes invasive behavior

To next directly analyze cooperative invasion between neuroblastoma subtypes that are seen in vivo, we prepared MCS consisting of S-type SHEP cells mixed with N-type cells. The invasive pattern of spheroids consisting of each cell type alone was compared with invasive patterns when S- and N-type cells were mixed, and this revealed a striking change in invasive behavior (Figure 2, A and B). Collagen-embedded S-type SHEP MCS display a single-cell invasion mode, with predominately elongated cells radiating out from the spheroid center. In contrast, N-type SH-SY-5Y MCS display a mixed mode of invasion, with both collectively invading strands and individually invasive cells. This changed to a predominantly individual cell invasion mode in mixed SHEP/SH-SY-5Y MCS (Figure 2, A and B). Even more strikingly, the N-type IMR32 MCS changed from a noninvasive phenotype into small clusters of invading cells in mixed SHEP/IMR32 MCS (Figure 2, A and B).

We confirmed that the invasive fractions in the mixed MCS indeed constituted representatives from each of the two subtypes by first labeling cells with alternative membrane-permeant fluorescent dyes to facilitate subtype detection within the mixed MCS. In each case, S-type SHEP cells were labeled with red fluorescent dye and N-type cells were labeled in green. Immediately after being embedded in 3D collagen (Figure 3, A and C, 0 h), green and red cells are observed mixed throughout the MCS. At 48 h later, mixed green and red cells are clearly visible throughout the invasive cell populations in both SHEP/SH-SY-5Y MCS (Figure 3A) and SHEP/IMR32 MCS (Figure 3C). The detection of IMR32 cells at the boundary of the invasive front was particularly striking, given the absence of IMR32 invasion when cultured alone (compare to Figure 2B). Of note, quantification of the extent of invasion revealed differences between the two sets of cultures. The SHEP cells invaded significantly further than the SH-SY-5Y cells in mixed SHEP/SH-SY-5Y MCS (Figure 3B). In contrast, SHEP and IMR32 cells invaded to the same extent as each other (Figure 3D). Moreover, the total distance invaded by the SHEP cells was reduced when in combination with the IMR32 versus when in combination with the SH-SY-5Y cells. We considered whether the invasive phenotype of the IMR32 cells might be due to poor spheroid compaction when cocultured with the SHEP cells. However, analysis of spheroid compaction confirmed that there is no difference between the compaction of IMR32 spheroids versus IMR32 spheroids cocultured with SHEP cells (Figure 3E).

The observation that the SHEP cells invade further than the SH-SY-5Y cells suggested that the SHEP cells might invade first from the mixed SHEP/SH-SY-5Y spheroid. Conversely, the equivalent invasion seen between the SHEP and IMR-32 cells suggested that the invasion of these two cell types from the MCS might be concurrent. To investigate these possibilities, we performed live imaging of the mixed MCS. Of importance, SHEP cells (labeled red) were the first to emerge from the SHEP/SH-SY-5Y mixed MCS, appearing ~4 h after embedding (Figure 4A). In contrast, SHEP and IMR-32 cells (red and green, respectively) emerge from the mixed MCS at the same time (see 12 h, Figure 4B). Note that the emergence of the SHEP cells from the SHEP/IMR-32 mixed MCS is delayed compared with the SHEP/SH-SY-5Y mixed MCS, in agreement with our observation of the reduced overall extent of SHEP invasion in SHEP/IMR-32 mixed MCS.

Mixed MCS invasion requires Rac

Owing to the striking induction of IMR32 invasion when mixed with SHEP cells, we focused on the mechanism behind this cooperative invasion. The concurrent emergence and extent of invasion by the

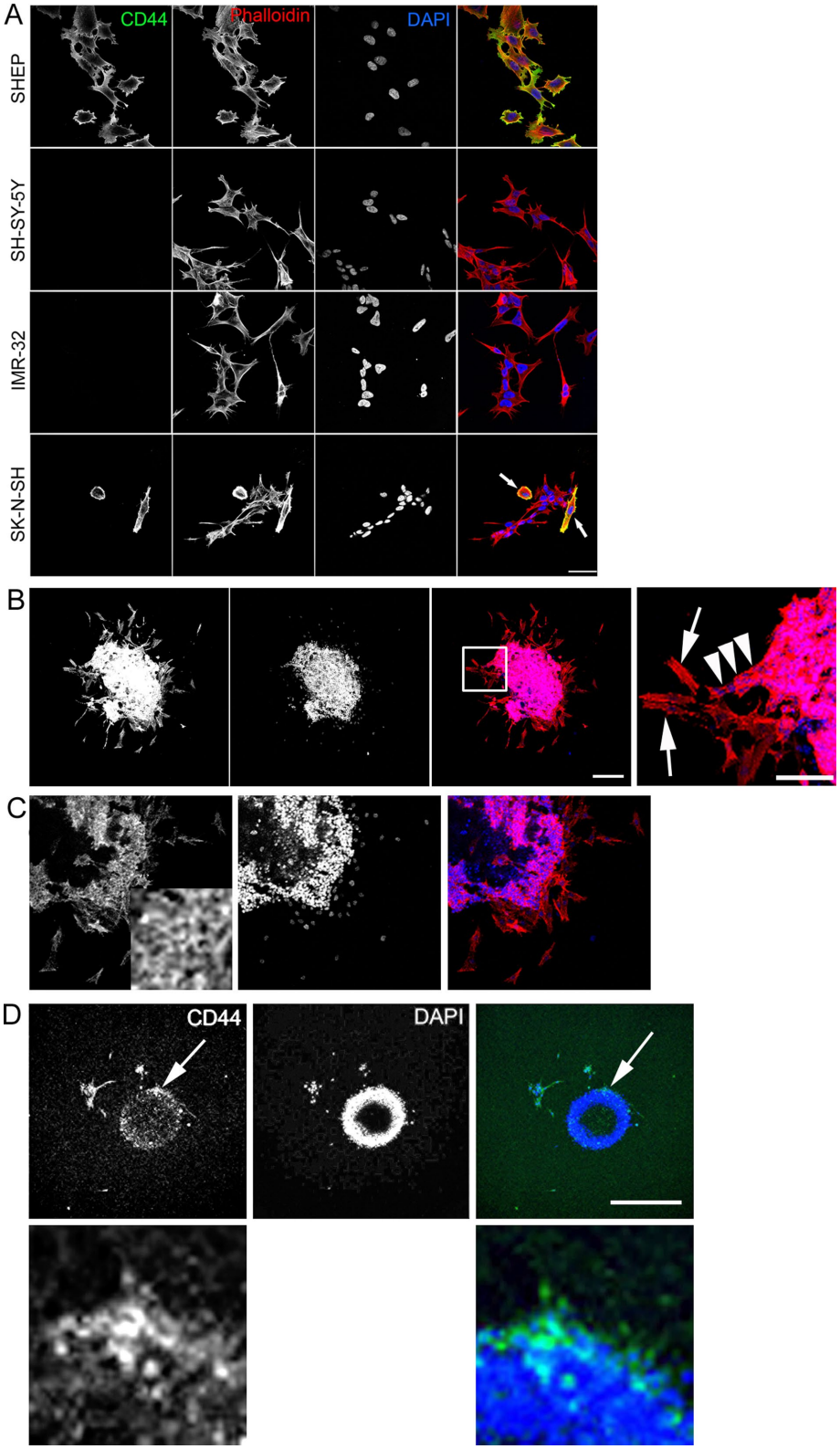

FIGURE 1: S-type cells have the phenotype of leader cells. (A) Immunostaining of SHEP, SH-SY-5Y, IMR-32, and SK-N-SH cells for CD44 (green), phalloidin (red), and DAPI (blue). CD44-positive cells are indicated with arrows. Scale bar, 50 μm. (B) Representative confocal images (maximum projection) of SK-N-SH cells grown as multicellular spheroids suspended in 3D collagen gels. Spheroids were incubated for 48 h after embedding in collagen and stained with phalloidin (left; red in merged image) and Hoechst (middle; blue in merged image). Scale bar, 250 μm. Right, magnification of the boxed region. Arrowheads indicate an invasive strand; arrows indicate individual, elongated invasive cells. Scale bar, 100 μm. (C) Single confocal slice of the SK-N-SH MCS showing detail of cobblestone phalloidin staining (magnified inset in the first image). (D) Maximum projection of SK-N-SH spheroids 48 h after embedding in collagen immunostained with CD44 antibody (green) and Hoescht (blue). Asterisks indicate individual invasive cells. Arrows indicate regions shown in magnified images. Scale bar, 500 μm.

SHEP and IMR32 cells from the mixed MCS and lack of collective strand invasion suggested a different mechanism from previously described follow-the-leader invasion (Gaggioli *et al.*, 2007; Carey *et al.*, 2013). We therefore first analyzed the role of Rac GTPase and Rho kinase in the mixed MCS invasion. We found that Rac inhibition (EHT 1864) efficiently blocks invasion in the mixed MCS (Figure 5A). Analysis of MCS in which cell lines were first differentially labeled with fluorescent dyes confirmed that Rac inhibition significantly inhibits invasion of both cell types within the mixed MCS (Figure 5, B–D). In contrast, both cell lines remain invasive when treated with the Rho kinase inhibitor Y-27632 (Figure 5, A–D). Invasion was efficiently inhibited by cotreatment with EHT 1864 and Y-27632. Thus the invasive phenotype induced in mixed SHEP/IMR32 MCS is Rac dependent and Rho kinase independent.

It is striking that Rac inhibition arrested IMR-32 invasion in the mixed MCS (Figure 5, B and D), given that IMR-32 cells have low Rac expression and activity (Mitchell and O'Neill, 2016). Conversely, S-type cells have high Rac activity and were previously shown to exhibit Rac-dependent invasion (Mitchell and O'Neill, 2016). Because neuroblastoma cells can be induced to differentiate into S-type phenotypes through exposure to bromodeoxyuridine (BrdU; Sugimoto *et al.*, 1988), we assessed whether BrdU-induced differentiation could stimulate IMR-32 invasion. Indeed, 48-h exposure to 10 μM BrdU induced invasion of IMR-32 spheroids (Figure 6). These data therefore confirm that differentiation can switch neuroblastoma cells to an invasive phenotype.

MMPs mediate SHEP incorporation between IMR32 cells

Because Rac-dependent invasion through 3D collagen gels is frequently accompanied by MMP activity (Friedl, 2004), we next tested the role of MMPs. We compared the effects of treatment with the broad-spectrum MMP inhibitor Marimastat/BB2516 and the specific MMP2 inhibitor oleylhydroxamic acid. Both inhibitors significantly

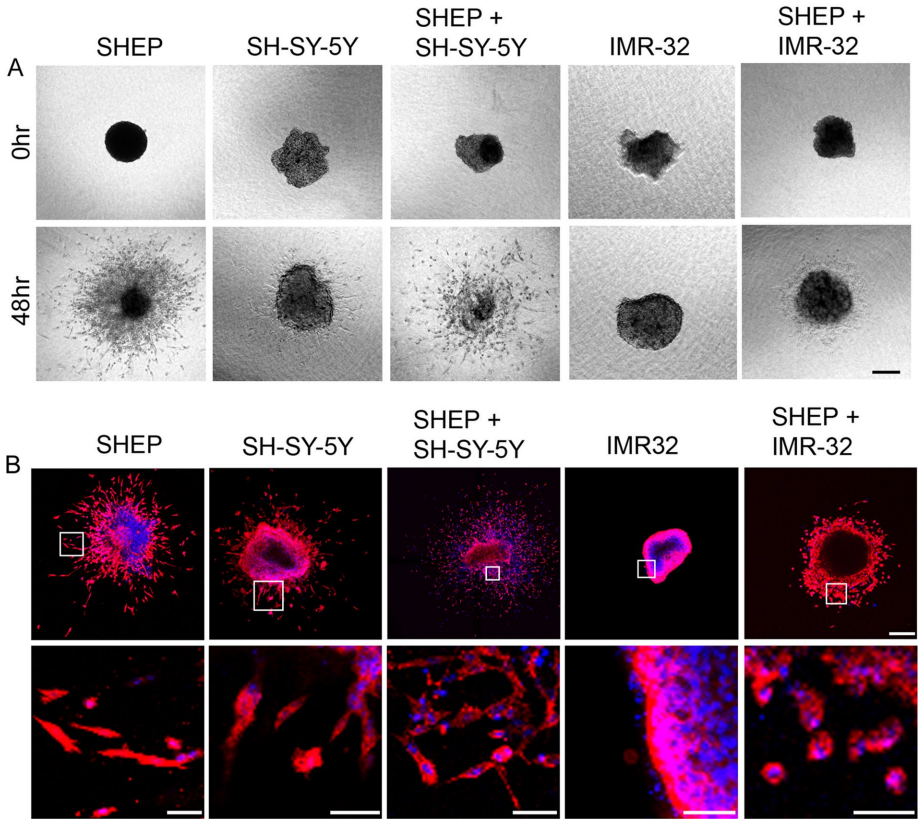

FIGURE 2: Mixed cultures exhibit different invasive phenotypes. (A) Bright-field images at 0 and 48 h of individual spheroids composed of a single cell line (SHEP, SH-SY-5Y, and IMR-32) and mixed spheroids (SH-SY-5Y+SHEP, and IMR-32+SHEP) embedded in 3D collagen gels. Scale bar, 200 µm. Data are representative of >22 spheroids over more than four individual experiments. (B) Confocal images (maximum projection) of individual (SHEP, SH-SY-5Y, and IMR-32) and mixed (SHEP + SH-SY-5Y; SHEP + IMR-32) spheroids 48 h after plating, stained with phalloidin (red) and Hoechst blue (blue). Zoomed-in regions indicated by white boxes. The zoomed regions represent single confocal slices in order to highlight the morphology of the invasive cells. Scale bars, 200 µm (top), and 50 µm (bottom). Representative spheroids were selected from more than nine spheroids over more than three individual experiments.

reduced the invasiveness of SHEP/IMR32 mixed MCS (Figure 7A), indicating that the invasion is MMP2 dependent. These results suggested that SHEP cells might use an MMP-dependent mode of invasion. However, when we analyzed the effect of MMP inhibition on the invasion of SHEP MCS alone, there was limited effect (Figure 7A), indicating that they invade in an MMP-independent manner. We then considered whether the SHEP cells might switch between MMP-independent amoeboid invasion to MMP-dependent invasion when cocultured with N-type cells. Our analyses revealed that cells in SHEP MCS have an elongated morphology (Figure 7B). Moreover, their invasion is Rac dependent but Rho kinase independent, as demonstrated by MCS response to Rac (EHT1864) and Rho kinase (Y-27632) inhibitors (Figure 7B). Therefore SHEP invasion does not confirm to established characteristics of amoeboid invasion, which is characterized by rounded cell shape and Rho kinase dependence (Sanz-Moreno *et al.*, 2008). Finally, we examined whether MMP inhibition similarly reduces SK-N-SH invasion. Indeed, we found that the pan-MMP inhibitor Marimastat/BB2516 causes a small but significant reduction in invasion (Figure 7C).

Our results revealed that MMPs are required for invasion in mixed SHEP/IMR32 MCS but not for invasion from SHEP MCS. In trying to reconcile these observations, we considered the fact that the distance that the SHEP cells invaded appeared reduced when cocultured with IMR32 cells versus their distance invaded when cultured alone. Comparison of the distances invaded confirmed that SHEP invasion is reduced when cocultured with IMR-32 cells (Figure 8A). Given the cell–cell adhesion exhibited by the IMR32 MCS, we considered whether the IMR32 cell–cell interactions presented a barrier to SHEP invasion. On the basis of previous reports that MMPs can cleave cell–cell adhesions (Grabowska and Day, 2012), we asked whether MMP activity might be required for SHEPs to break through the barrier presented by IMR32 cell–cell adhesion. To test this, we adapted a previous method for analyzing the incorporation of one cell type into layers of a second cell type (Hamilla *et al.*, 2014). IMR32 cells were grown to high confluence, and SHEP cells were then introduced to the cultures. After fixation, SHEP cells were identified by immunostaining with CD44 antibodies. The location of individual SHEP cells relative to the IMR32 cell layer was then determined using orthogonal projections of confocal *z*-stacks (Figure 8, B–D). Incorporated SHEP cells (middle) are those that reside within the IMR32 layers and are surrounded in all directions by IMR32 cells (Figure 8C). Unincorporated SHEP cells are those located either on top of the IMR32 cells or below the IMR32 cells (Figure 8, B and D). Quantification revealed that under control conditions, 45.8 ± 3.2% of SHEP cells were incorporated into the IMR32 cell layer (Figure 8E). Live imaging of fluorescently tagged SHEP cells after introduction to the confluent IMR32 cultures confirmed that the SHEP cells actively invade between IMR32 cells (Figure 8F). Next we tested whether MMP inhibition blocked SHEP incorporation into IMR32 cell clusters. On treatment with BB2516 or MMP2 inhibitor, the number of incorporated SHEP cells significantly decreased to 22.3 ± 1.0% ($p < 0.0001$) and 9.7 ± 2.1% ($p < 0.0001$), respectively (Figure 8E). These results reveal that MMP activity promotes SHEP incorporation between IMR32 cells. We therefore propose that in the mixed SHEP/IMR32 MCS, MMP activity is required for SHEP cells to insert between IMR32 cells.

DISCUSSION

Our study revealed that S-type neuroblastoma cells can influence the invasion patterns of N-type neuroblastoma cells and vice versa. We showed that S-type cells switch N-type SH-SY-5Y cells into a predominantly single-cell invasion mode, whereas they induce invasion of small cell clusters from otherwise noninvasive N-type IMR32 spheroids. Concurrently, coculture with N-type cells reduces the extent of S-type invasion. We show that SHEP induction of IMR32 requires MMP activity and that this facilitates SHEP insertion between IMR32 cells. Thus we demonstrate mutual effects on invasion between the two cell types.

Of interest, we found that SHEP cells induce invasion either by single cells or by small cell clusters. This is contrast with other studies, in which cooperative invasion leads to the induction of collective

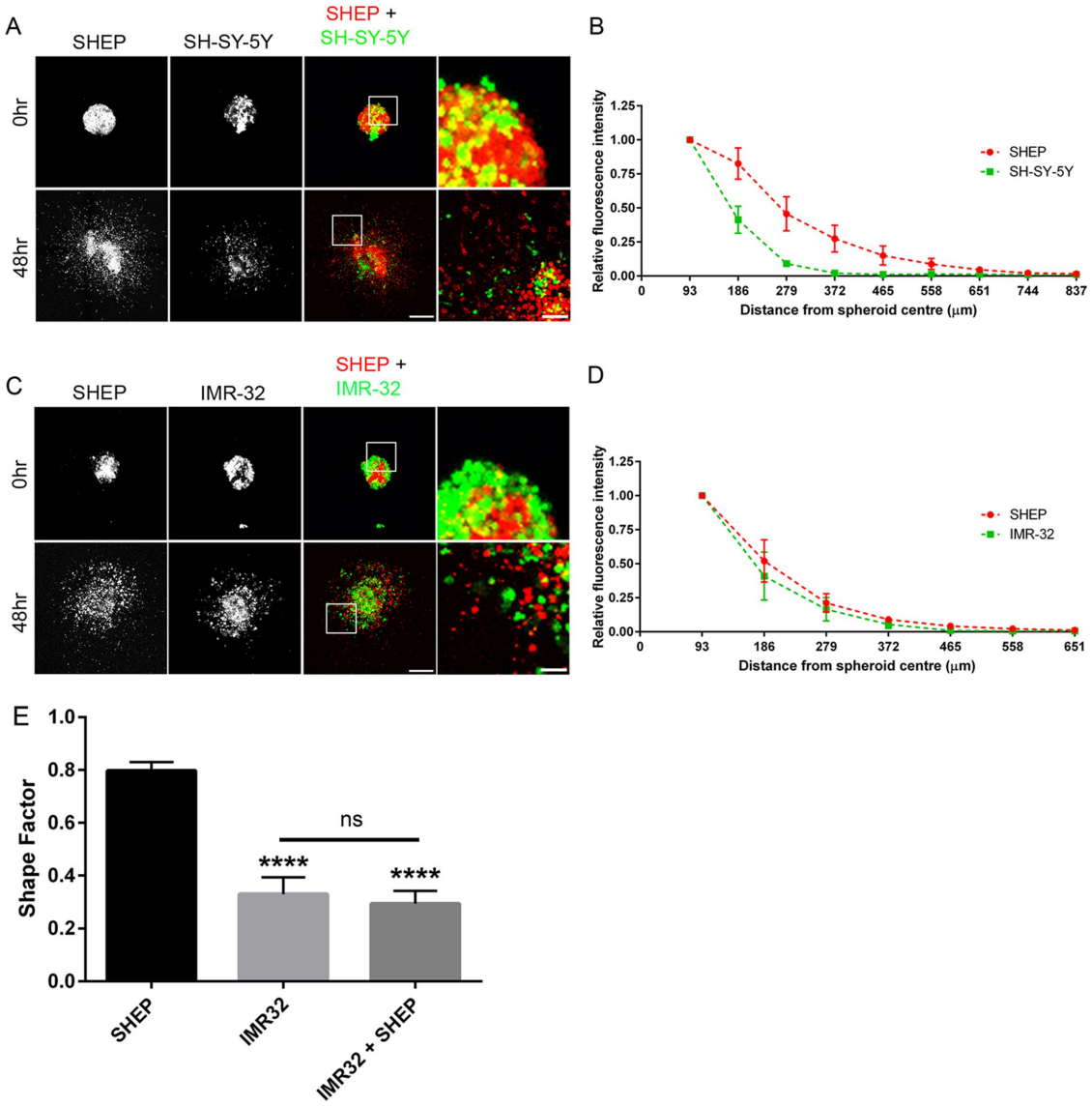

FIGURE 3: S-type cells induce invasion of N-type cells. (A, C) Representative confocal images (maximum projection) of cell tracker–labeled SHEP (red) plus (A) SH-SY-5Y (green) or (C) IMR32 (green) mixed spheroids at 0 and 48 h of incubation. Scale bar, 300 μm (main images), 50 μm (far right, zoomed images). (B, D) Quantification of spheroid invasion of each cell line within the mixed spheroid. SHEP, red; (B) SH-SY-5Y, green; (D) IMR32, green. Data are the average of >10 spheroids from three individual experiments. Error bars represent SEM. SHEP cells invade further than SH-SY-5Y cells: $p < 0.0001$, two-way analysis of variance (ANOVA). SHEP and IMR32 cells invade to the same distance: p = ns, nonsignificant, two-way ANOVA. (E) Shape factor of spheroids before embedding in collagen. Shape factor of 1.0 is equivalent to a perfect circle. ****$p < 0.0001$.

strand invasion (Gaggioli *et al.*, 2007; Carey *et al.*, 2013; Cheung *et al.*, 2013; Westcott *et al.*, 2015) or an invasive file of cells (Chapman *et al.*, 2014). This may reflect cell type–dependent behaviors, given the tendency for different tumor types to disseminate via single-cell or collective-migration mechanisms (Friedl and Wolf, 2003), although our demonstration of collective strand invasion in the SK-N-SH MCS suggests that this mode of invasion is available to neuroblastoma cells.

Our data demonstrate that when cocultured with SHEP cells, IMR-32 cells exhibit Rac-dependent invasion. Of importance, this effect is phenocopied by incubation with BrdU. This treatment was previously shown to induce neuroblastoma cells to differentiate into S-type phenotypes (Sugimoto *et al.*, 1988). Therefore the IMR-32 cell switch to Rac-dependent invasion suggests that coculture with S-type SHEP cells may induce IMR-32 differentiation. There are a number of potential mechanisms that may explain this. First, the SHEP cells may secrete a soluble factor that induces N-type differentiation. However, conditioned media from SHEP cells failed to induce IMR-32 invasion (unpublished data). Alternatively, direct cell–cell contact between the two cell subtypes may induce IMR32 differentiation in the 3D environment. It is also possible that changes to the matrix environment brought about by invasive SHEP cells may change the matrix-derived signals received by the IMR-32 cells, which in turn may induce differentiation.

Our results suggested that coculture with IMR-32 cells switches S-type cells to MMP-mediated invasion. Other studies demonstrated similar results to those in the present study, in which invasion of poorly invasive melanoma cells was induced by highly invasive

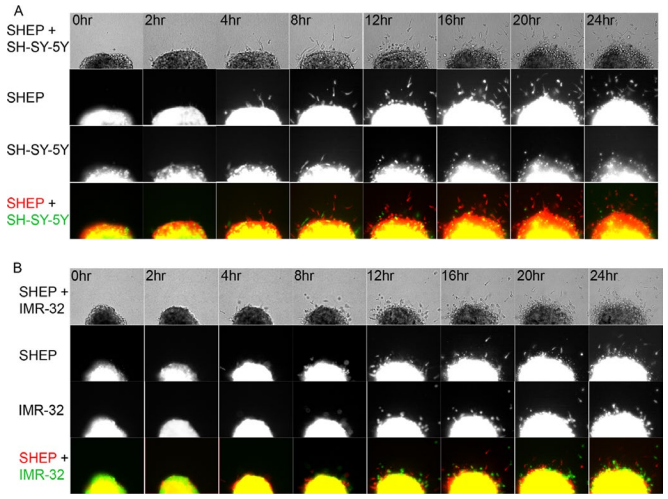

FIGURE 4: Time-lapse imaging of mixed MCS. (A) Representative montage of time-lapse images of mixed SHEP/SH-SY-5Y MCS over a 24-h time period. SHEP cells in red and SH-SY-5Y cells in green. (B) Mixed SHEP/IMR32 spheroids labeled and imaged as in A. Representative spheroids from nine individual spheroids over three independent experiments.

melanoma cells (Alexander and Friedl, 2012). In common with our results, MMP inhibition blocked cooperative invasion of mixed invasive and poorly invasive melanoma spheroids but had no effect on the invasive cells when cultured alone as spheroids. However, in contrast to our results, the coculture of the melanoma cell types induced the invasive cells to switch from an amoeboid, MMP-independent invasion to mesenchymal MMP-dependent invasion. We found no such transition in the SHEP cells. Instead, our data suggest that the MMPs are required for SHEP cells to insert between the IMR32 cells. Of note, when cultured as spheroids embedded in 3D collagen gels, the IMR32 cells exhibit tight cell–cell adhesions, indicated by the striking cobblestone appearance of the actin. Indeed in 2D culture, N-type neuroblastoma cells are characterized by their propensity for increased intracellular adhesion (Ross *et al.*, 2003). Thus we propose that the IMR-32 cells create a barrier for SHEP invasion and that MMPs are required for SHEP cells to pass through the tight cell–cell adhesions of the IMR32 cells. Of importance, MMP inhibition did not completely abrogate invasion. We interpret this result to mean that the SHEP cells on the edges of the spheroids, and thus not blocked by an IMR32 barrier, were free to invade the matrix. It is not possible to discern from our experiments whether the MMP activity is derived from the SHEP or IMR32 cells, and in future, it will be interesting to determine this.

Our results expand the known mechanisms of cooperative invasion, revealing mutual effects on invasion between two neuroblastoma cell subtypes. An important question is whether this is unique to neuroblastoma cells or whether examination of cells of different tumor origins may reveal that this

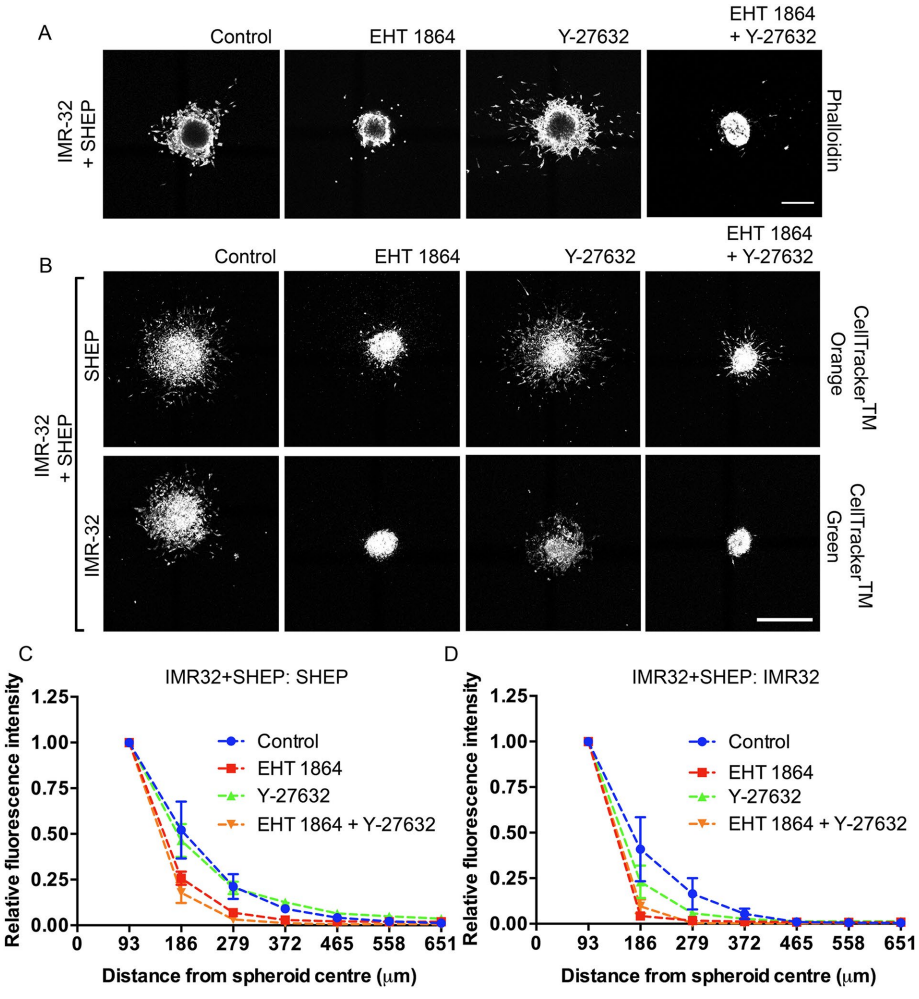

FIGURE 5: SHEP induction of IMR-32 invasion is Rac dependent. (A) Representative confocal images (maximum projection) of IMR-32/SHEP mixed spheroids after 48 h of incubation. Treatments with EHT 1864, Y-2732, and a combination. Cells were fixed and stained with phalloidin. Scale bar, 500 μm. (B) Representative confocal images (maximum projection) of IMR-32/SHEP mixed spheroid invasion. Individual cell lines are labeled with alternative fluorescent CellTracker dyes, with each cell line displayed separately as black and white images (top, SHEP; bottom, IMR-32). Spheroids were treated with EHT 1864, Y-27632, and a combination and fixed after 48 h. Scale bar, 500 μm. (C) Quantification of SHEP cell invasion in the mixed SHEP/IMR32 spheroids under the treatment conditions indicated. Data are the average of more than six individual spheroids from more than three individual experiments. Error bars represent SEM. Control vs. EHT1864, $p = 0.0012$; control vs. Y-27632, ns; control vs. combination, $p < 0.0001$; two-way ANOVA. (D) IMR32 invasion in the mixed SHEP/IMR32 spheroids under the treatment conditions indicated. Data are the average of more than six individual spheroids from more than three individual experiments. Error bars represent SEM. Control vs. EHT1864, $p < 0.0001$; control vs. Y-27632, ns; control vs. combination, $p = 0.0012$; two-way ANOVA.

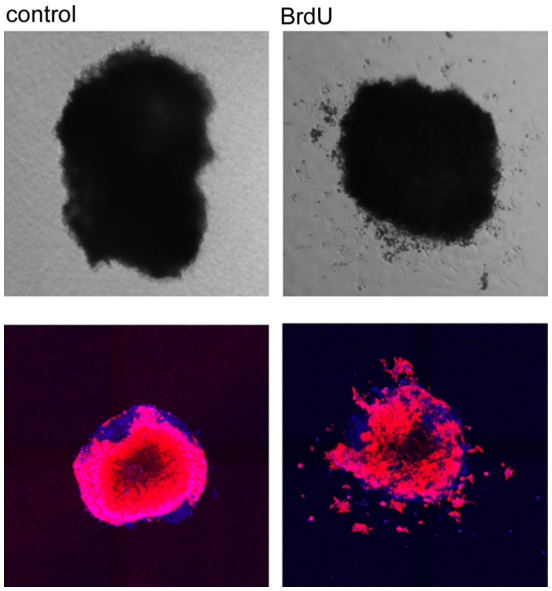

FIGURE 6: BrdU treatment induces IMR32 invasion. Top, bright-field images of control and BrdU (10 μM)–treated IMR32 spheroids. Bottom, maximum projections of IMR32 spheroid (vehicle control) vs. IMR32 cells treated with BrdU to induce differentiation. Spheroid cultures stained to reveal actin (red) and nuclei (blue).

mechanism exists in other tumor backgrounds. It is particularly interesting that S-type and N-type cells have been identified in a percentage of metastatic neuroblastoma tumors in bone (Valent *et al.*, 1999, 2001). Potentially, the different invasive phenotypes induced by cooperative invasion of mixed cell subtypes may influence the route of dissemination and eventual metastasis. In the search for new approaches to treating invasive cancers, it is critical to understand the role of each member of heterogeneous populations making up the primary tumor in the eventual tumor dissemination. Defining these mechanisms will help to identify the correct cells for targeting and the relevant signaling pathways for new treatments.

MATERIALS AND METHODS

Cell lines and cell culture

Cultured neuroblastoma cell lines (SH-EP, SK-N-SH, IMR-32, SH-SY-5Y) were kindly provided by Loretta Lau (Kids Research Institute, Sydney, Australia). Cell lines were maintained in DMEM supplemented with 10% fetal bovine serum (FBS; vol/vol). SH-SY-5Y cells were maintained in MEM/F12 supplemented with 10% FBS (vol/vol) and 1% nonessential amino acids (vol/vol).

Three-dimensional multicellular spheroid invasion assay

To generate spheroids, cells were first seeded on 0.8% agarose–coated 96-well plates in media and incubated at 37°C for 48 h. The nonadhesive surface of the agarose induces the cells to compact together to form a spheroid. After 48 h of compaction, spheroids were embedded in collagen gels, following published protocols (Lees *et al.*, 2011; Zhong *et al.*, 2014). Briefly, spheroids were resuspended in 1.7 mg/ml collagen solution (collagen type I, rat tail [354236; Corning, Sydney, Australia] and neutralizing buffer [phosphate-buffered saline (PBS), 100 mM 4-(2-hydroxyethyl)-1-piperazineethanesulfonic acid]) and allowed to polymerize at 37°C for 1 h. After gel polymerization, complete medium with or without pharmacological agents was

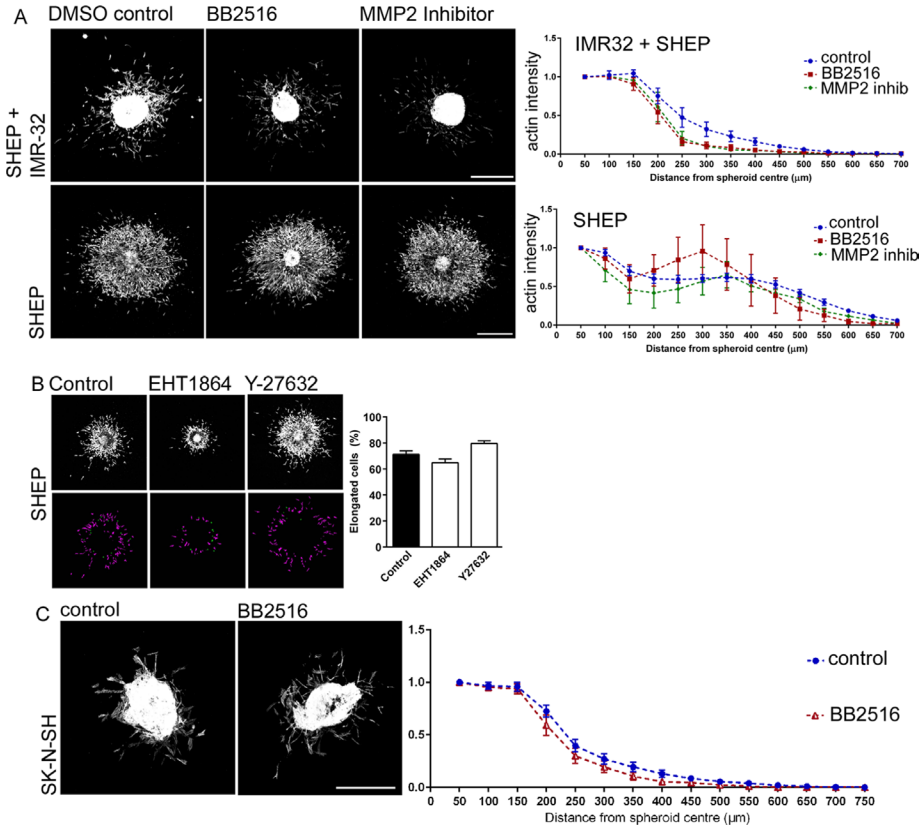

FIGURE 7: MMPs mediate mixed IMR32/SHEP invasion. (A) Representative confocal images (maximum projection) of SHEP and IMR32/SHEP mixed spheroids after 48 h of incubation. Treatments with BB2516 (100 μM) and MMP2 inhibitor (50 μM). Spheroids were fixed and stained with phalloidin. Scale bars, 500 μm. Graphs show quantification of spheroid invasion of IMR32/SHEP mixed MCS and SHEP MCS under the indicated treatment conditions. Data are the average of more than six individual spheroids from more than three individual experiments. Error bars represent SEM. IMR32/SHEP mixed spheroids: control vs. BB2516, $p = 0.0001$; control vs. MMP2 inhibitor, $p = 0.0016$. SHEP spheroids: control vs. BB2516, ns; control vs. MMP2 inhibitor, $p = 0.0093$. Two-way ANOVA. (B) Representative confocal images (maximum projection) of SHEP spheroids embedded in collagen after 48 h of incubation. Treatments with EHT 1864 and Y-27632. Cells were fixed and stained with phalloidin (top) and then thresholded for cell shape and false colored (elongated, purple; round, green). Histograms show the percentage of individual elongated cells (bottom). Data are from more than seven spheroids, from at least three independent experiments. (C) Representative confocal images (maximum projection) of SK-N-SH spheroids treated with BB2156 (100 μM) as indicated. Graph shows quantification of SK-N-SH spheroid invasion. Data are from a minimum of 10 spheroids per condition. Error bars represent SEM. Control vs. BB2516, $p = 0.0143$; two-way ANOVA.

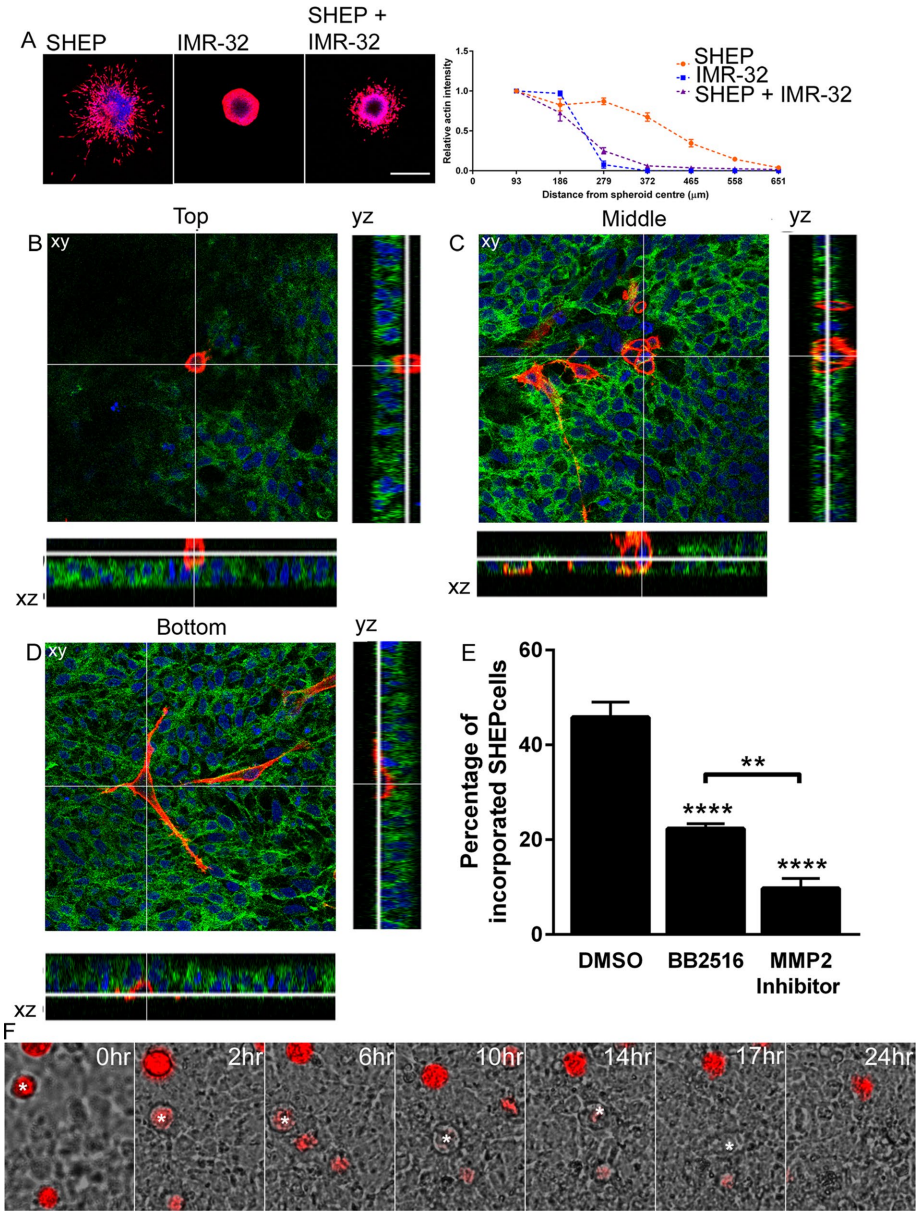

FIGURE 8: MMP mediates SHEP incorporation into IMR32 layers. (A) Representative confocal images of the indicated single and mixed spheroids. Right, graph showing the extent of spheroid invasion for each of the conditions. (B–D) Orthogonal projections of representative examples of top- (B), middle- (C), and bottom- (D) located SHEP cells. Projections of *xy*, *yz*, and *xz* are shown to reveal cell location through the *z*-stack. Cells were immunostained with phalloidin (green) and DAPI (blue) and counterstained with CD44 (red) to identify the SHEP cells. (E) Percentage of SHEP cells incorporated into the IMR32 layers. Data are pooled from two technical replicates (183–519 individual cells counted per replicate) from three individual biological experiments. ****$p < 0.0001$ compared with DMSO control; **$p < 0.01$ indicated by line. (F) Representative montage of time-lapse images of red-labeled SHEP cells incorporating into layers of IMR32 cells over a 24-h time period. Asterisks indicate the SHEP cell of interest.

added, and spheroids were incubated for 48 h. To facilitate comparison between cells lines, initial experiments were carried out to determine the numbers of each cell line required to provide similar-sized spheroids at the time of initial plating (unpublished data). Mixed spheroids were also generated from two different cell types. To allow differentiation between cell lines, individual cell lines were labeled with 10 μM CellTracker orange CMRA dye (Life Technologies, Melbourne, Australia) or 10 μM CellTracker green CMFDA dye (Life Technologies) in serum-free medium for 2 h before being detached with trypsin. The two alternatively labeled cells lines (SHEP plus SH-SY-5Y or IMR-32) were then mixed together (1:1 ratio), seeded onto agarose-coated 96-well plates in complete medium, and incubated at 37°C for 48 h. Resulting spheroids were then embedded in collagen gels. After 1 h of gel polymerization, either medium or medium plus inhibitors was added, and cultures were incubated for a further 48 h. The pharmacological agents used were 10 μM Y-27632 (Tocris, Bristol, United Kingdom), 25 μM EHT-1864 (Tocris), 100 μM BB2516 (Tocris), and 50 μM MMP2 inhibitor oleylhydroxamic acid (Calbiochem, San Diego, CA).

Immunofluorescence

For immunofluorescence of cells grown on coverslips, 0.5×10^5 to 1×10^5 cells were plated onto collagen (50 μg/ml)-coated glass coverslips and cultured for 24 h. Cells were fixed in 4% paraformaldehyde (PFA) and permeabilized in 0.2% Triton X-100 in PBS. After blocking in PBS containing 1% bovine serum albumin (BSA), cells were incubated with CD44 antibody (Cell Signaling Technology, Boston, MA), Alexa Fluor 488–conjugated secondary antibody (Invitrogen), tetramethylrhodamine isothiocyanate (TRITC)–phalloidin (Sigma-Aldrich, Sydney, Australia), and 4′,6-diamidino-2-phenylindole (DAPI; Sigma-Aldrich) nuclear stain. Coverslips were mounted using Calbiochem Fluorsave reagent (Merck Millipore, Sydney, Australia). Fluorescence imaging was performed on a Leica SP5II confocal microscope with a 63× oil objective. Spheroids embedded in 3D collagen gels were fixed with 4% PFA and treated with 0.15 M glycine in PBS to quench background fluorescence. Spheroids were then permeabilized in 0.2% Triton X-100 in PBS and blocked in PBS containing 1% BSA and 1% donkey serum. Collagen-embedded spheroids were incubated with a combination of CD44 antibody, TRITC-phalloidin, and Hoescht blue nuclear stain and stored in PBS for imaging. Confocal *z*-stack imaging was performed on a Leica SP5 II confocal microscope with a 10× air objective, and maximum projection and analyses were performed using Leica LAS and MetaMorph (version 7.7) software.

Incorporation assay

IMR32 cells were seeded at a density of 0.8×10^6 cells per glass coverslip and grown for 72 h. After 72 h, SHEP cells were seeded on top of the near-confluent IMR32 coverslips at a density of 0.2×10^6 cells per coverslip. The SHEP cells were seeded in medium containing dimethyl sulfoxide (DMSO), BB2516 (100 μM), or MMP2 inhibitor (50 μM). Coverslips were incubated for a further 24 h. Cells were then fixed in 4% PFA, blocked in 5% donkey serum/0.5% BSA, and permeabilized in 0.2% Triton X-100 in PBS. Cells were examined for

immunofluorescence following the foregoing protocol, with CD44 labeled with an Alexa Fluor 594–conjugated antibody. Confocal *z*-stack imaging and tile scanning were performed on a Leica SP5 II confocal microscope with a 63× oil objective. Orthogonal projections of stacks were made in MetaMorph software, each individual CD44-positive cell was counted, and stack location was determined as bottom, middle, or top. Middle cells represent cells that incorporated into the IMR32 cell layer, with bottom cells located below and top cells on or above the IMR32 cell layer.

Analysis and image preparation

Integrated morphometry analysis of cell morphology was carried out with MetaMorph software (version 7.7). Cell shape was quantified by calculating the shape factor (values of 1 indicating a perfect circle). Spheroid images were first filtered to remove the central spheroid core, thereby allow thresholding of individual migrating cell shape factor in an automated manner. Cells with a shape factor <0.75 were scored as elongated, and those with a shape factor between 0.75 and 1.0 were scored as round. Thresholded images were binarized and false-colored green (rounded cells) and purple (elongated cells). Concentric circle analysis was carried out with ImageJ software. A series of concentric circles (16 circles, inner radius of 30, outer radius of 484) was overlaid on spheroid images, and the average pixel intensity along the perimeter of each circle was calculated. All spheroids were normalized to the average pixel intensity of the inner circle. Densitometric analysis was achieved with ImageJ. Statistical analyses were performed in GraphPad Prism. Final images and grayscale adjustments were prepared in Adobe Photoshop.

ACKNOWLEDGMENTS

We gratefully acknowledge the assistance of Loretta Lau and Rebecca Dagg in the sourcing and growth of the neuroblastoma lines and Laurence Cantrill for assistance with imaging. This work was generously supported by a Childhood Cancer Cytoskeleton Consortium (C4) Fellowship from The Kids' Cancer Project to C.M.

REFERENCES

Alexander S, Friedl P (2012). Cancer invasion and resistance: interconnected processes of disease progression and therapy failure. Trends Mol Med 18, 13–26.

Carey SP, Starchenko A, McGregor AL, Reinhart-King CA (2013). Leading malignant cells initiate collective epithelial cell invasion in a three-dimensional heterotypic tumor spheroid model. Clin Exp Metastasis 30, 615–630.

Chapman A, Fernandez del Ama L, Ferguson J, Kamarashev J, Wellbrock C, Hurlstone A (2014). Heterogeneous tumor subpopulations cooperate to drive invasion. Cell Rep 8, 688–695.

Cheung KJ, Gabrielson E, Werb Z, Ewald AJ (2013). Collective invasion in breast cancer requires a conserved basal epithelial program. Cell 155, 1639–1651.

Ciccarone V, Spengler BA, Meyers MB, Biedler JL, Ross RA (1989). Phenotypic diversification in human neuroblastoma cells: expression of distinct neural crest lineages. Cancer Res 49, 219–225.

Dang TT, Prechtl AM, Pearson GW (2011). Breast cancer subtype-specific interactions with the microenvironment dictate mechanisms of invasion. Cancer Res 71, 6857–6866.

DeNardo DG, Barreto JB, Andreu P, Vasquez L, Tawfik D, Kolhatkar N, Coussens LM (2009). CD4(+) T cells regulate pulmonary metastasis of mammary carcinomas by enhancing protumor properties of macrophages. Cancer Cell 16, 91–102.

Etienne-Manneville S (2014). Neighborly relations during collective migration. Curr Opin Cell Biol 30, 51–59.

Friedl P (2004). Prespecification and plasticity: shifting mechanisms of cell migration. Curr Opin Cell Biol 16, 14–23.

Friedl P, Wolf K (2003). Tumour-cell invasion and migration: diversity and escape mechanisms. Nat Rev Cancer 3, 362–374.

Gaggioli C, Hooper S, Hidalgo-Carcedo C, Grosse R, Marshall JF, Harrington K, Sahai E (2007). Fibroblast-led collective invasion of carcinoma cells with differing roles for RhoGTPases in leading and following cells. Nat Cell Biol 9, 1392–1400.

Giampieri S, Manning C, Hooper S, Jones L, Hill CS, Sahai E (2009). Localized and reversible TGFbeta signalling switches breast cancer cells from cohesive to single cell motility. Nat Cell Biol 11, 1287–1296.

Grabowska MM, Day ML (2012). Soluble E-cadherin: more than a symptom of disease. Front Biosci (Landmark Ed) 17, 1948–1964.

Gross N, Beretta C, Peruisseau G, Jackson D, Simmons D, Beck D (1994). CD44H expression by human neuroblastoma cells: relation to MYCN amplification and lineage differentiation. Cancer Res 54, 4238–4242.

Hamilla SM, Stroka KM, Aranda-Espinoza H (2014). VE-cadherin-independent cancer cell incorporation into the vascular endothelium precedes transmigration. PLoS One 9, e109748.

Lees JG, Bach CTT, Bradbury P, Paul A, Gunning PW, O'Neill GM (2011). The actin-associating protein Tm5NM1 blocks mesenchymal motility without transition to amoeboid motility. Oncogene 30, 1241–1251.

Mitchell CB, O'Neill GM (2016). Rac GTPase regulation of 3D invasion in neuroblastomas lacking MYCN amplification. Cell Adh Migr, doi: 10.1080/19336918.2016.1183868.

Mora J, Cheung NK, Juan G, Illei P, Cheung I, Akram M, Chi S, Ladanyi M, Cordon-Cardo C, Gerald WL (2001). Neuroblastic and Schwannian stromal cells of neuroblastoma are derived from a tumoral progenitor cell. Cancer Res 61, 6892–6898.

Mora J, Gerald WL (2004). Origin of neuroblastic tumors: clues for future therapeutics. Expert Rev Mol Diagn 4, 293–302.

Ross RA, Biedler JL, Spengler BA (2003). A role for distinct cell types in determining malignancy in human neuroblastoma cell lines and tumors. Cancer Lett 197, 35–39.

Sanz-Moreno V, Gadea G, Ahn J, Paterson H, Marra P, Pinner S, Sahai E, Marshall CJ (2008). Rac activation and inactivation control plasticity of tumor cell movement. Cell 135, 510–523.

Sugimoto T, Kato T, Sawada T, Horii Y, Kemshead JT, Hino T, Morioka H, Hosoi H (1988). Schwannian cell differentiation of human neuroblastoma cell lines in vitro induced by bromodeoxyuridine. Cancer Res 48, 2531–2537.

Thiele CJ (1998). Neuroblastoma cell lines. Human Cell Culture, Vol. 1, Lancaster, United Kingdom: Kluwer, 21–53.

Valent A, Benard J, Venuat AM, Silva J, Duverger A, Duarte N, Hartmann O, Spengler BA, Bernheim A (1999). Phenotypic and genotypic diversity of human neuroblastoma studied in three IGR cell line models derived from bone marrow metastases. Cancer Genet Cytogenet 112, 124–129.

Valent A, Venuat AM, Danglot G, Da Silva J, Duarte N, Bernheim A, Benard J (2001). Stromal cells and human malignant neuroblasts derived from bone marrow metastasis may share common karyotypic abnormalities: the case of the IGR-N-91 cell line. Med Pediatr Oncol 36, 100–103.

Westcott JM, Prechtl AM, Maine EA, Dang TT, Esparza MA, Sun H, Zhou Y, Xie Y, Pearson GW (2015). An epigenetically distinct breast cancer cell subpopulation promotes collective invasion. J Clin Invest 125, 1927–1943.

Wyckoff JB, Wang Y, Lin EY, Li JF, Goswami S, Stanley ER, Segall JE, Pollard JW, Condeelis J (2007). Direct visualization of macrophage-assisted tumor cell intravasation in mammary tumors. Cancer Res 67, 2649–2656.

Zhong J, Bach CT, Shum MS, O'Neill GM (2014). NEDD9 regulates 3D migratory activity independent of the Rac1 morphology switch in glioma and neuroblastoma. Mol Cancer Res 12, 264–273.